PCCP

PAPER

View Article Online
View Journal | View Issue



Cite this: *Phys. Chem. Chem. Phys.*, 2016, **18**, 10563

# $C_\beta$–H stretching vibration as a new probe for conformation of *n*-propanol in gaseous and liquid states†

Yuanqin Yu,[a] Yuxi Wang,[b] Naiyin Hu,[b] Ke Lin,[b] Xiaoguo Zhou[b] and Shilin Liu*[b]

The development of potential probes to identify molecular conformation is essential in organic and biological chemistry. In this work, we investigated a site-specific C–H stretching vibration as a conformational probe for a model compound, 1,1,3,3,3-deuterated *n*-propanol ($CD_3CH_2CD_2OH$), using stimulated photoacoustic Raman spectroscopy in the gas phase and conventional spontaneous Raman spectroscopy in the liquid state. Along with quantum chemistry calculations, the experiment shows that the $CH_2$ symmetric stretching mode at the β-carbon position is very sensitive to the conformational structure of *n*-propanol and can serve as a new probe for all five of its conformers. Compared with the O–H stretching vibration, a well-established conformational sensor for *n*-propanol, the $C_\beta$–H stretching vibration presented here shows better conformational resolution in the liquid state. Furthermore, using this probe, we investigated the conformational preference of *n*-propanol in pure liquid and in dilute water solution. It is revealed that in pure liquid, *n*-propanol molecules prefer the *trans*-OH conformation, and in dilute water solution, this preference is enhanced, indicating that the water molecules play a role of further stabilizing the *trans*-OH *n*-propanol conformers. This leads to conformational evolution that *n*-propanol molecules with *gauche*-OH structure are transferred to the *trans*-OH structure upon diluting with water. These results not only provide important information on structures of *n*-propanol in different environments, but also demonstrate the potential of the C–H stretching vibration as a new tool for conformational analysis. This is especially important when considering that hydrocarbon chains are structural units in organic and biological molecules.

Received 13th January 2016,
Accepted 13th March 2016

DOI: 10.1039/c6cp00244g

www.rsc.org/pccp

## Introduction

Molecular conformation is an important aspect in chemistry and biology since the properties and functions of many organic and biological molecules depend significantly on their conformational structure, which is determined by a subtle balance between intramolecular and intermolecular interactions. In the past few decades, much attention has been paid to developing experimental and theoretical methods to infer conformational structure at the molecular level. The combinations of various spectroscopic techniques with quantum chemistry calculations have allowed us to directly characterize the conformation of flexible molecules in the gas phase.[1–4] Particularly, infrared (IR)–UV spectroscopy, UV–UV hole-burning spectroscopy, ionization-loss stimulated Raman spectroscopy and the chirality-sensitive microwave three-wave mixing technique have been demonstrated to be powerful tools for probing individual conformers of biomolecules.[5–15]

Besides experimental and theoretical methods, the development of potential sensors to identify molecular conformation is also essential. It is known that vibrational spectroscopy is a versatile tool for conformational analysis since different conformers have distinct signatures in observed spectra. Historically, the vibrational spectra of many functional groups, such as −CO, −OH and −NH groups, have been well established as a conformational probe of organic molecules.[16–19] In contrast, −CH groups have not yet been widely employed although they exist commonly in organic molecules. As a matter of fact, the C–H stretching region is of special usefulness. It is highly localized without significant mixing with other vibrational modes, and exhibits relatively strong intensity in both IR and Raman measurements. In order to make a definite assignment in the C–H stretching region, the Strauss group have carried out a series of benchmark studies on alkane systems using low-temperature Raman spectroscopy and successfully interpreted complex

[a] *School of Physics and Material Science, Anhui University, Hefei, Anhui 230039, China*
[b] *Hefei National Laboratory for Physical Sciences at the Microscale, iChEM (Collaborative Innovation Center of Chemistry for Energy Materials), Department of Chemical Physics, University of Science and Technology of China, Hefei 230026, China. E-mail: slliu@ustc.edu.cn*

† Electronic supplementary information (ESI) available. See DOI: 10.1039/c6cp00244g

spectral features in the C–H stretching region with the inclusion of Fermi coupling between stretching vibrations and bending overtones.[20–22] Their results have been generally used in subsequent studies. Nowadays, the development of the C–H stretching region as a probe of molecular structures continues to be an area of considerable interest, as shown in recent experimental and theoretical studies by several research groups.[8,9,23–27] In this study, we investigated Raman spectra of a simple model compound, *n*-propanol, in the C–H stretching region, and present clear experimental evidence that the C–H stretching vibration is sensitive to conformational change of a flexible molecule. Our experimental result is in good agreement with recent theoretical studies that the site-specific C–H stretching vibrations exhibit remarkable sensitivity to the backbone conformation of protein and peptide molecules.[28–31]

The backbone of *n*-propanol ($CH_3CH_2CH_2OH$) consists of three carbon atoms together with a hydroxyl group, as illustrated in Fig. 1. It possesses two torsional degrees of freedom, CCCO and CCOH, leading to five distinguishable conformers. *n*-Propanol has been considered to be a valuable testing model for conformational investigation. Its conformational assignment has been the subject of numerous studies using a variety of experimental and theoretical methods.[19,32–45] The analyses of pure rotational spectra of *n*-propanol and its –OD isotopologue led to the identification of two conformers.[32,33] Recently, with a combination of contemporary broadband microwave spectroscopy and high-level quantum calculation, Kisiel *et al.* established unambiguous assignments to the complex rotational transitions of all five conformers, and stated that the $G_t$ conformer is the most stable form in gaseous *n*-propanol.[36] Using vibrational spectroscopy, two stable conformers of *n*-propanol, *trans*-OH and *gauche*-OH, were reported from a pulsed high-throughput nozzle FTIR spectrometer.[37] Later, Jarmelo *et al.* studied the low-temperature matrix-isolation IR absorption spectrum, and tentatively assigned the observed O–H stretching spectra to five conformers.[39] Liu *et al.* studied the cavity ring down spectrum in the region of O–H stretching overtones, and interpreted it by considering the contributions of five conformers.[38] Very recently, Wasserman *et al.* studied the gas-phase IR absorption spectra and Raman spectra of *n*-propanol under supersonic jet cooling conditions, and presented a first complete assignment of the observed O–H stretching fundamental spectra to five conformers.[41,42] While it has been verified that the O–H stretching vibration can be used as a good conformational probe for different conformers of gaseous *n*-propanol, there are no reports on the C–H stretching vibration. This may be due to the fact that *n*-propanol contains several C–H groups, which results in severe spectral overlapping in the C–H stretching region. Therefore, it is relatively hard to make a clear assignment in the C–H stretching region.

For molecules containing several –CH groups, it is well known that isotope substitution is an effective way to eliminate spectral interferences from different –CH groups, and then a site-specific –CH or –CD group can be selected. In the present work, a deuterated compound, $CD_3CH_2CD_2OH$, was employed to investigate the sensitivity of the $C_\beta$–H stretching vibration toward conformations of *n*-propanol using gas-phase Raman spectroscopy. An important advantage of gas-phase Raman spectroscopy is that the spectra exhibit narrow and separated band shapes, allowing for better conformational resolution than broad rovibrational profiles present in IR spectra. This is due to the facts that the Raman selection rules emphasize the sharp Q-branches over the broader $\Delta J \neq 0$ branches while the band centers should remain the same in the IR and Raman measurements This advantage makes gas-phase Raman spectroscopy a powerful tool for conformational analysis. Unfortunately, Raman signals are generally weak in the gas phase, especially for liquid samples with low vapor pressures such as *n*-propanol studied here. For this reason, we use a sensitive nonlinear spectral technique, called stimulated photoacoustic Raman spectroscopy (PARS), to record vibrational spectra of gaseous $CD_3CH_2CD_2OH$ in the C–H stretching region. Quantum chemistry calculations were employed to aid the assignment of observed spectra.

Additionally, considering that the *n*-propanol molecule is often chosen as a model system for biological molecules, the investigation of conformational structures in pure liquid or solution states is also quite important to elucidate its

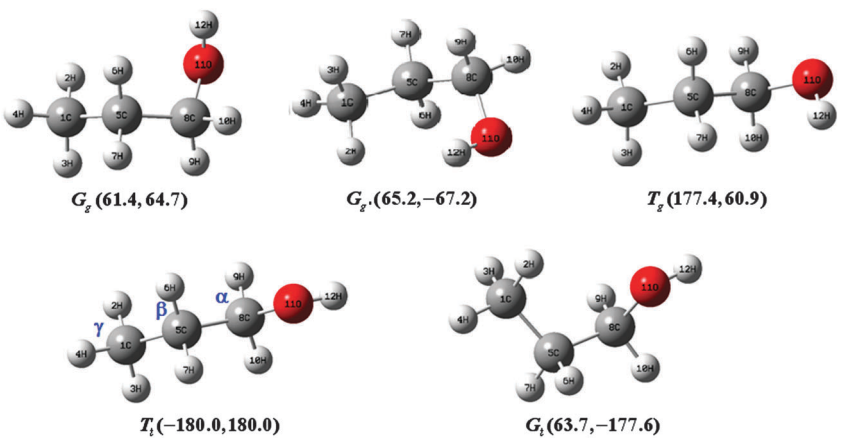


Fig. 1 The optimized geometries for five conformers of *n*-propanol at B3LYP/6-311++G(d,p) levels. The values of two dihedral angles, CCCO and CCOH, are shown in parentheses.

 

conformational stability against environmental changes and the interactions from solvent molecules, thus yielding important insight into biological systems. In this work, based on the $C_\beta$–H stretching vibration, we investigated conformational preference and structural change of *n*-propanol in pure liquid state and in dilute aqueous solution by measuring Raman spectra of liquid $CD_3CH_2CD_2OH$. Compared with the O–H stretching vibration, the advantage of the $C_\beta$–H stretching vibration is that the hydrogen-bonding networks formed in liquid *n*-propanol have less impact on its band broadening, and thus conformation information can still be retained. On the contrary, the spectral features from different conformations are washed out in the O–H stretching region due to severe band broadening caused by hydrogen-bond interaction, which limits the O–H stretching vibration as a conformation probe for liquid *n*-propanol, especially in pure liquid and in water solution. Therefore, from this aspect, the C–H stretching vibration has greater potential for conformational analysis of organic and biological molecules in different environments.

## Experimental and computational methods

Deuterated *n*-propanol, $CD_3CH_2CD_2OH$, was purchased from ICON isotopes, whose purity was checked by gas chromatography (GC) and was found to be more than 99%. Normal *n*-propanol ($CH_3CH_2CH_2OH$) was obtained from Sigma-Aldrich (>99.8%, GC grade).

### Polarized PARS

The basic theory and experimental setup of PARS have been fully described in previous papers,[46–53] but to be complete, a short description is included here. When the frequency difference between two laser beams (pump and Stokes beams) is resonant with a Raman-active vibrational transition, a stimulated Raman scattering process occurs and the ground-state molecules are transferred to vibrationally excited states. Then collisions cause the excitation energy to be converted into local heating, which creates a sound wave that is detected by a microphone. The sensitivity of PARS is greatly increased in contrast to direct measurement of weak Raman scattering photons. The PARS intensity can be expressed as

$$I \propto I_P I_s(\cos^2\theta + \rho \sin^2\theta) \quad (1)$$

where $I_P$ and $I_s$ are the intensities of pump and Stokes laser beams, respectively, $\rho$ is the Raman depolarization ratio, and $\theta$ is the cross angle between the polarization directions of the two laser beams. It can be seen that $\rho$ can be accurately determined by recording PARS intensity as a function of the angle $\theta$. More straightforwardly, the PARS intensity ratio at $\theta = 90^\circ$ and $\theta = 0^\circ$ is the depolarization ratio, where $\theta = 90^\circ$ and $\theta = 0^\circ$ mean that the polarization directions of the two laser beams are orthogonal and parallel to each other, respectively. In the present study, the values of $\rho$ were obtained by fitting the $I$–$\theta$ curve with eqn (1) because it is more accurate.[47]

In the experiment, the second-harmonic output of 532.1 nm from a pulsed Nd:YAG laser (line width 1.0 $cm^{-1}$, pulse width 10 ns) was split into two beams by a quartz wedge. About 90% of the 532.1 nm laser energy directly entered into a dye laser system (ND6000, line width 0.05 $cm^{-1}$) for generating a tunable Stokes beam (625–637 nm), and the remainder was used as a pump beam for PARS. The two linearly polarized laser beams were focused in the center of a photoacoustic cell in a counterpropagating configuration. The photoacoustic signal is monitored by an oscilloscope to obtain the PARS intensity or averaged by a boxcar integrator to obtain a PARS spectrum. The energies of the pump and Stokes beams are typically 10 and 6 mJ per pulse, respectively. The sample pressure is kept at 5 Torr. The obtained PARS spectrum is normalized to the intensity of the Stokes beam, and the wavelengths of both beams are calibrated by a wavelength meter with an accuracy of 0.005 nm. The change of cross angle between polarization directions of the two laser beams is controlled by a rotatable half-wave plate in the pump beam. The measured precision of the depolarization ratio is checked by the $\nu_1$ (2917 $cm^{-1}$) and $\nu_3$ (3020 $cm^{-1}$) vibrational modes of methane with an accuracy of 0.005.

### Liquid Raman spectroscopy

The Raman spectra of $CD_3CH_2CD_2OH$ in pure liquid state and in dilute aqueous solutions are recorded in a conventional spontaneous Raman experiment. The instrument and setup parameters are similar to those reported previously.[17,54–56] Briefly, all the experimental data were collected with a triple monochromator system (Acton Research, TriplePro) connected to a liquid-nitrogen-cooled CCD detector (Princeton Instruments, Spec-10:100B). The excitation light (4 W power) was from a stable cw laser (Coherent, Verdi-V5, 532 nm). The Raman shifts of the spectra were calibrated with the standard lines of a mercury lamp, and the spectral resolution was ~1.0 $cm^{-1}$. During the measurement of temperature-changed liquid Raman spectra, a heating bath (THD-2006, Ningbo) was used to control the temperature (±0.1 °C) of the samples in a 10 × 10 mm quartz cuvette. The *n*-propanol aqueous solutions were prepared by mass measurement of *n*-propanol and triply distilled water to achieve the desired molar concentrations.

### Calculation details

All calculations were performed with the Gaussian 09 suite of programs at density functional theory (DFT) B3LYP (Becke, three-parameter, Lee–Yang–Parr) and MP2 (second-order Møller–Plesset perturbation) levels of theory using standard 6-311++G(d,p) basis set,[57] including geometry optimizations, relative energies and harmonic vibrational frequencies. To obtain a detailed interpretation of fundamental modes, the potential energy distribution (PED%) is calculated using freeware GAR2PED written by Martin and Alsenoy, a program to obtain a potential energy distribution from a Gaussian archive record.[58] To assist the analysis of the experimental spectra, all the calculated frequencies from the B3LYP/6-311++G(d,p) method were scaled down by a factor of 0.973 for the C–H stretching and bending regions, and a factor of 0.957 for the O–H stretching region,[48–50] while a factor

of 0.956 was applied for the C–H stretching region calculated at the MP2/6-311++G(d,p) level.[39] The details of the frequencies, Raman activities, depolarization ratio, PED analysis and mode descriptions for five conformers of deuterated and normal *n*-propanol in selected spectral region are summarized in Tables S1 and S2 (ESI†), including C–H bending region (1400–1500 $cm^{-1}$), C–H stretching region (2800–3100 $cm^{-1}$) and O–H stretching region (3600–3700 $cm^{-1}$). It is noted that only the results from the B3LYP method are listed in Tables S1 and S2 (ESI†) since the B3LYP method is demonstrated to give satisfactory results in spectroscopic studies, especially for organic molecular systems, and the calculations of the MP2 method give similar results. To obtain the simulated Raman spectra, the calculated Raman activities ($S_i$) and depolarization ratios ($\rho_i$) were used to evaluate the Raman intensities ($I_i$) of the $i$th vibrational mode according to the following equation:[13,59]

$$I_i = \frac{f(\nu_0 - \nu_i)^4 S_i}{\nu_i(1+\rho_i)[1-\exp(-hc\nu_i/kT)]} \quad (2)$$

where $\nu_0$ is the excitation wavenumber in $cm^{-1}$, $\nu_i$ is the vibrational wavenumber of the $i$th normal mode, $c$ is the speed of light, $T$ is the temperature, $h$ and $k$ are Planck's and Boltzmann's constants, respectively, and $f$ is a normalization factor for all peak intensities.

# Results and discussion

### Calculated structure and relative energy

The optimized geometries of five conformers of *n*-propanol are shown in Fig. 1, and labeled as $G_g$, $G_{g'}$, $T_g$, $T_t$ and $G_t$, respectively. In the notation used here, the uppercase letters (G and T) refer to the orientation of the CCCO rotational axis and the lowercase letters ($t$ and $g$) to the orientation of the CCOH rotational axis; G and $g$ = *gauche* (60°), and T and $t$ = *trans* (180°); the prime (′) indicates a negative value for the corresponding dihedral angles of CCCO and CCOH. Among the five conformers, $G_g$, $G_{g'}$, $T_g$ and $G_t$ come in enantiomeric pairs and are spectroscopically and energetically indistinguishable from their mirror images $G'_g$, $G'_{g'}$, $T_{g'}$ and $G'_t$, respectively. Thus, all of these four conformers have statistical abundances equal to 2, whereas only the $T_t$ conformer has a statistical abundance equal to 1.

Table 1 summarizes the relative energy of the five conformers for $CD_3CH_2CD_2OH$ calculated at the DFT (B3LYP) and MP2 levels, with the $G_t$ conformer being chosen as the zero of energy. Due to the small energy difference between the five conformers, the energy ordering was found to be dependent on levels of theory in previous studies.[36,39,40,45] Here, the energy sequences of the five conformers are also not systematic between B3LYP and MP2 levels, as seen from Table 1. As a result of these energy differences, it is expected that all five conformers should be significantly populated at room temperature and therefore contribute to the observed spectra. For comparison with deuterated *n*-propanol, the relative energies of the five conformers of normal *n*-propanol ($CH_3CH_2CH_2OH$) calculated at both the B3LYP and MP2 levels are also listed in Table 1. It is clear that isotope substitution has a negligible influence on the energy order of the five conformers.

Table 1 The calculated relative energy $\Delta E_{ZPE}$ (kJ $mol^{-1}$) corrected by zero-point energy (ZPE) for five conformers of deuterated and normal *n*-propanol

| | | B3LYP/6-311++G(d,p) | | MP2/6-311++g(d,p) | |
|---|---|---|---|---|---|
| Molecule | Conformer | ZPE | $\Delta E_{ZPE}$ | ZPE | $\Delta E_{ZPE}$ |
| $CD_3CH_2CD_2OH$ | $G_t$ | 240.79 | 0 | 245.22 | 0 |
| | $T_t$ | 240.75 | 0.04 | 244.52 | 0.75 |
| | $T_g$ | 241.11 | 0.25 | 245.91 | 1.5 |
| | $G_g$ | 241.04 | 0.62 | 245.88 | 1.33 |
| | $G_{g'}$ | 241.08 | 1.13 | 245.69 | 2.01 |
| $CH_3CH_2CH_2OH$ | $G_t$ | 283.51 | 0 | 288.74 | 0 |
| | $T_t$ | 283.38 | −0.04 | 287.89 | 0.63 |
| | $T_g$ | 283.88 | 0.34 | 289.42 | 1.54 |
| | $G_g$ | 283.90 | 0.75 | 289.47 | 1.42 |
| | $G_{g'}$ | 283.86 | 1.17 | 289.24 | 2.03 |

Table 2 The calculated frequencies ($cm^{-1}$) of $C_\beta H_2$ symmetric and antisymmetric stretching for five conformers of $CD_3CH_2CD_2OH$ molecule

| | B3LYP/6-311++G(d,p)[a] | | MP2/6-311++g(d,p)[b] | |
|---|---|---|---|---|
| Conformation | $C_\beta H_2$ symm. str. | $C_\beta H_2$ anti-symm. str. | $C_\beta H_2$ symm. str. | $C_\beta H_2$ anti-symm. str. |
| $T_t$ | 2950 | 2983 | 2954 | 3006 |
| $G_t$ | 2940 | 2973 | 2943 | 2994 |
| $G_{g'}$ | 2936 | 2974 | 2941 | 2995 |
| $T_g$ | 2923 | 2972 | 2931 | 2992 |
| $G_g$ | 2918 | 2952 | 2924 | 2976 |

[a] Scale factor of 0.973. [b] Scale factor of 0.956.

Table 2 lists the frequencies of the $C_\beta H_2$ symmetric and antisymmetric stretching modes of $CD_3CH_2CD_2OH$ at B3LYP and MP2 levels of theory. It can be seen that both stretching vibrations exhibit large frequency variability among the five conformers, sensitive to structural changes of *n*-propanol molecules. The maximum frequency difference is about 32 $cm^{-1}$ at both theoretical levels. It should be stressed that, in a rigid sense, the use of symmetric and antisymmetric stretching is only appropriate to describe two $C_\beta$–H bond stretching vibrations of the $T_t$ conformer, and is not suitable for the other four conformers. We also note that the vibrations of these two modes are highly localized in the $CD_3CH_2CD_2OH$ molecule. Moreover, they carry symmetric and antisymmetric stretching characters with in-phase and out-of-phase $C_\beta$–H bond vibrations, respectively, as presented in PED analysis (Table S1, ESI†). Therefore, for convenience of description, we temporarily use symmetric and antisymmetric stretching to label these two modes of the other four conformers.

### Gas-phase Raman spectra in the C–H stretching region

The polarized and depolarized Raman spectra of gaseous $CD_3CH_2CD_2OH$ in the C–H stretching region from 2800 to 3000 $cm^{-1}$ have been respectively recorded with PARS for both parallel ($\theta$ = 0°) and perpendicular ($\theta$ = 90°) polarization configurations and are presented in Fig. 2. It can be seen that the polarized spectrum exhibits complex features in the C–H

 

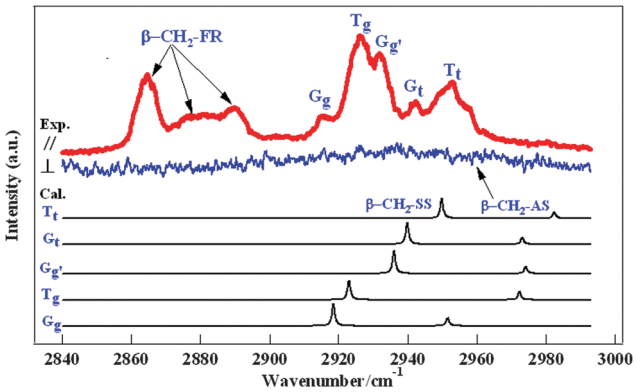


Fig. 2 Polarized and depolarized PARS spectra of gaseous $CD_3CH_2CD_2OH$ in the C–H stretching region measured under parallel (∥) and perpendicular (⊥) laser polarization configurations, respectively. The calculated fundamental Raman spectra for five conformers in the C–H stretching region at the B3LYP/6-311++G(d,p) level are also plotted. $CH_2$-SS: $CH_2$ symmetric stretching; $CH_2$-FR: $CH_2$ Fermi resonance; $CH_2$-AS: $CH_2$ antisymmetric stretching.

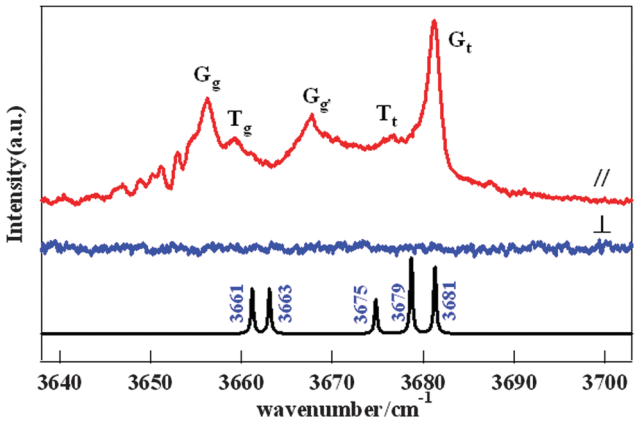


Fig. 3 Polarized and depolarized PARS spectra of gaseous normal *n*-propanol ($CH_3CH_2CH_2OH$) in the O–H stretching region measured under parallel (∥) and perpendicular (⊥) laser polarization configurations, respectively. The calculated O–H stretching Raman spectrum for five conformers at B3LYP/6-311++G(d,p) level is also plotted.

stretching region, consisting of two distinct parts. One is the high-energy region from 2900 to 2960 $cm^{-1}$, and the other is the low-energy region from 2850 to 2900 $cm^{-1}$. In the high-energy region, five distinct bands at 2952, 2942, 2932, 2926 and 2915 $cm^{-1}$ can be clearly resolved. Among them, the bands at 2952 and 2926 $cm^{-1}$ are more intense than those at 2942, 2932 and 2915 $cm^{-1}$. For the low-energy region, three bands at 2865, 2880 and 2889 $cm^{-1}$ can be observed. The depolarized spectrum exhibits only one weak and broad band in the range 2900–2980 $cm^{-1}$. To aid the assignment of observed spectra, Raman depolarization ratios of all bands in polarized spectra were determined according to the $I$–$\theta$ curve method mentioned above, and are summarized in Table 3. It can be seen that the measured depolarization ratios are very small compared to the value of 0.75, indicating that these bands are strongly polarized and belong to symmetric modes.

## Conformational assignment

In comparison to the experimental spectra, the calculated fundamental and Raman intensities of $C_\beta H_2$ symmetric and antisymmetric stretching modes of $CD_3CH_2CD_2OH$ are convolved with a Lorentzian function (FWHW 1.0 $cm^{-1}$) to obtain the simulated spectra of each conformer in the C–H stretching region, as shown in Fig. 2. Combining with the depolarization ratio measurement, we assigned the high-energy bands at 2952, 2942, 2932, 2926 and 2915 $cm^{-1}$ to the $C_\beta H_2$ symmetric stretching vibration (β-$CH_2$-SS) of the five conformers $T_t$, $G_t$, $G_{g'}$, $T_g$ and $G_g$, respectively, as labeled in Fig. 2 and summarized in Table 3. It can be seen that the observed maximum frequency difference of β-$CH_2$-SS is ~37 $cm^{-1}$, in agreement with theoretical prediction that the $C_\beta$–H stretching vibration exhibits sensitivity towards conformational structures of *n*-propanol. As hydrocarbon chains are important structural units in organic and biological molecules, the experimental results presented here provide the promise for application to a larger range of flexible molecules. It should be mentioned that the assigned band for $T_t$ conformer seems to be comprised of two shoulders and one strong band. We attribute it to the rotational structures in the Q-branch of $T_t$ conformer since similar structures are also observed in the O–H stretching region, as shown in Fig. 3.

Table 3 The spectral assignment of gaseous $CD_3CH_2CD_2OH$ in the C–H stretching region

| Observed position ($cm^{-1}$) | Depolarization ratio ($\rho$) | Assignment |
|---|---|---|
| 2865 | 0.060 | β-$CH_2$-FR |
| 2880 | 0.100 | β-$CH_2$-FR |
| 2889 | 0.089 | β-$CH_2$-FR |
| 2915 | 0.230 | $T_t$-β-$CH_2$-SS |
| 2926 | 0.108 | $G_t$-β-$CH_2$-SS |
| 2932 | 0.113 | $G_{g'}$-β-$CH_2$-SS |
| 2942 | 0.210 | $T_g$-β-$CH_2$-SS |
| 2952 | 0.096 | $G_g$-β-$CH_2$-SS |
| Broad band (2900–2980) | | β-$CH_2$-AS |

For the low-energy bands at 2865, 2880 and 2889 $cm^{-1}$, we assign them to the $C_\beta H_2$ bending overtones, which are enhanced due to a Fermi resonance interaction with the $C_\beta H_2$ symmetric stretching vibrations. As listed in Table S1 (ESI†), the calculated bending modes are at 1460, 1439, 1438, 1457 and 1443 $cm^{-1}$ for the five conformers $T_t$, $G_t$, $G_{g'}$, $T_g$ and $G_g$, respectively, leading to the bending overtones lying very close to the symmetric stretching fundamental. Thus a Fermi resonance is expected between them. We denote these enhanced bending overtones as β-$CH_2$-FR. However, the bending overtones are not resolved like the fundamentals and the strong band at 2865 $cm^{-1}$ should be an overlap of two or three bending overtones.

In Fig. 2, the weak and broad feature in the depolarized spectrum ranging from 2900 to 2980 $cm^{-1}$ can be attributed to the $C_\beta H_2$ antisymmetric stretching (β-$CH_2$-AS) vibrations of five conformers of $CD_3CH_2CD_2OH$. This is consistent with the theoretical prediction in the simulated spectra and the general case that the antisymmetric band is very weak in Raman measurement whereas strong in IR.[60] The broad feature of the depolarized spectrum can be explained by the fact that

the depolarized band consists of $\Delta J = 0, \pm1, \pm2$ rotational transitions in the Raman measurement, whereas the polarized one consists primarily of $\Delta J = 0$ transitions. From the above assignment, it is clear that the asymmetric stretching is nearly degenerate with $C_\beta H_2$ symmetric stretching, different from harmonic calculation that the frequencies of symmetric stretching are lower than those of antisymmetric one, as listed in Table 2. This is due to the fact that Fermi coupling pushes the $C_\beta H_2$ symmetric stretching to shift to higher energy, while the bending overtones are pushed to lower energy.

Besides conformational assignment, there are some interesting features in the observed spectrum shown in Fig. 2. Firstly, the *g*-configured conformers, which contain a *gauche* OH group and comprise the $T_g$, $G_g$ and $G_{g'}$ conformers, are located at lower wavenumber, whereas the *t*-configured conformers, which contain a *trans* OH group and consist of the $G_t$ and $T_t$ conformers, are located at higher wavenumber. Secondly, a closer examination of the observed spectrum reveals that Raman intensities of conformers from the G family, including the three members $G_t$, $G_g$ and $G_{g'}$, are much lower than those from the T family, consisting of two members $T_g$ and $T_t$. This behavior of Raman transition intensities differing between G and T families was also observed in gas-phase Raman spectra of normal *n*-propanol in the O–H stretching region, as shown in Fig. 3. According to the calculated positions and previous assignment in supersonic expansion conditions, five distinct bands at 3681, 3676, 3668, 3659 and 3656 $cm^{-1}$ can be assigned to the conformers $G_t$, $T_t$, $G_{g'}$, $T_g$ and $G_g$, respectively. Some fine spectral structures located in the low-frequency part for the $G_g$ conformer can be attributed to rotational transitions since they disappear under supersonic expansion conditions.[33,34] It is evident that, like the C–H stretching region, the discrimination between different conformers of *n*-propanol is straightforward in the O–H stretching region, but the conformers from G family are much stronger than those from T family. In previous studies, similar behavior was also reported for the tryptamine molecule, which has nine conformers classified into three families.[3,14] It was shown that different members of each family have similar properties, but these properties differ significantly from one family to another. An example of such a property is the rotational constants of the conformers that are similar among the different members of a particular family, but different considerably between different families.[3]

It can be seen that in both C–H and O–H stretching regions, the predicted spectra provide a support for conformational assignments. However, for the prediction of reliable Raman intensity, they are not satisfactory, as seen from Fig. 2 and Fig. 3. As a matter of fact, the accurate prediction of Raman intensity is still one of the challenges of contemporary computational chemistry, especially in the C–H stretching region, in which Fermi coupling perturbs the intensity distribution.[61,62] Recently, some research groups have developed computational methods for addressing anharmonic vibrational calculation.[23–26,62] For example, the Sibert group developed a first-principles model for accurately describing the Fermi resonance coupling in the alkyl CH stretching region based on a local mode Hamiltonian that incorporates cubic stretch-bend coupling. They tested their models on several hydrocarbons systems, and excellent agreement is found between the predicted IR spectrum and observed single-conformation spectrum under supersonic cooling conditions.[23–26] Therefore, further theoretical works will be stimulated to describe the Raman intensity distribution and give detailed understanding of intramolecular interactions, such as Fermi coupling, in both C–H and O–H stretching regions of *n*-propanol.

Despite the fact that the observed and predicted intensity is not matched in the C–H and O–H stretching regions, further analysis seems to show that the B3LYP method can give reasonable prediction of Raman intensity of the conformers from the same G or T family, separately. Firstly, for the G family, the calculation indicated that the O–H stretching vibration of $G_t$ member is the strongest, whereas that of $G_{g'}$ member the weakest. This is well matched with the observation in the O–H stretching region, as shown in Fig. 3. On the other hand, in the C–H stretching region, the calculated $C_\beta H_2$ symmetric stretching of the $G_{g'}$ conformer is slightly stronger than those of $G_g$ and $G_t$ conformers. This is also the case in the experimental spectrum, as shown in Fig. 2. Secondly, for the T family, the calculations show that the $C_\beta H_2$ symmetric stretching vibration of the $T_t$ member is 1.1 times stronger than that of the $T_g$ member. However, the statistical abundance ratio between the $T_g$ and $T_t$ conformers leads to the observation that the $T_g$ conformer is nearly two times stronger than the $T_t$ conformer, as seen from Fig. 2. In the O–H stretching region, the $T_t$ conformer is 1.6 times stronger than the $T_g$ conformer according to the calculations. Also, the different statistical abundance ratio makes the $T_g$ conformer stronger.

### Conformational preference of liquid *n*-propanol

Compared with many investigations on conformations of gaseous *n*-propanol, no adequate interpretation of the conformations of liquid *n*-propanol has yet been given due to the lack of a suitable tool with the ability to discriminate its different conformations. In recent work using neutron scattering and X-ray diffraction techniques, it was suggested that in pure liquid state, *n*-propanol molecules in hydrogen-bond clusters probably prefer the *gauche* conformation with average dihedral angle CCCO of $\sim 77^\circ$, whereas for the orientation of another dihedral angle, CCOH, the information is very limited.[43,44,63] Here, we will show that temperature-dependent Raman spectra of liquid $CD_3CH_2CD_2OH$ in the C–H stretching region can provide valuable information on this aspect.

Fig. 4(a) presents the Raman spectrum of liquid $CD_3CH_2CD_2OH$ in the C–H stretching region at room temperature. To be contrasted, the spectrum in the O–H stretching region is also shown in Fig. 4(b). It is clear that the bands in both spectral regions are broadened due to the O–H$\cdots$O hydrogen-bond interactions in liquid *n*-propanol. However, different from the O–H stretching region, where the band is broadened to be a single one without any conformational structure, the information on conformations of liquid *n*-propanol can still be retained in the C–H stretching region.

According to gas-phase assignment in the C–H stretching region, the band at 2943 $cm^{-1}$ can be attributed to the *t*-configured

 

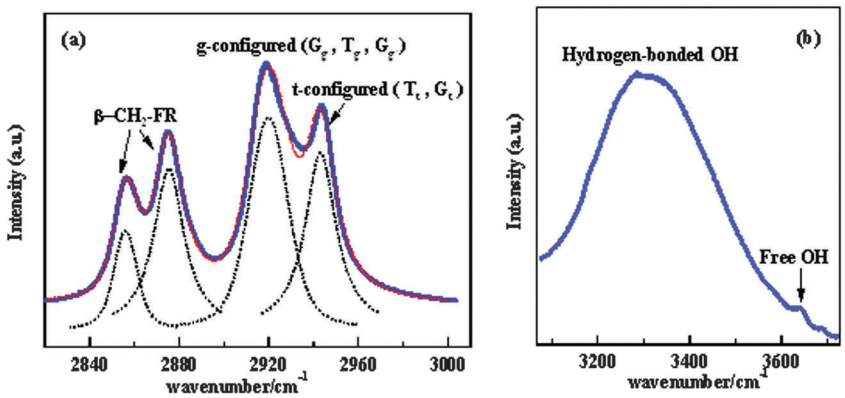


Fig. 4 Raman spectra of liquid $CD_3CH_2CD_2OH$ at room temperature: (a) the C–H stretching region (the thin red line is the fitted result using four Voigt profiles); (b) the O–H stretching region.

conformers, which contain *trans*-OH group and consist of $T_t$ and $G_t$ conformers, whereas the most intense band at 2920 $cm^{-1}$ can be attributed to the *g*-configured conformers, which contain *gauche*-OH group and comprise $T_g$, $G_g$ and $G_{g'}$ conformers, as labeled in Fig. 4(a). The other two bands at 2858 and 2875 $cm^{-1}$ are from Fermi resonance. Therefore, unlike gaseous *n*-propanol, the five conformers are no longer well assigned to particular bands in pure liquid state, but they are bunched into two groups with specific OH orientation, *trans*-OH and *gauche*-OH, respectively.

To determine relative stability of *t*-configured and *g*-configured conformers, the temperature-dependent Raman spectra of liquid $CD_3CH_2CD_2OH$ were measured at a series of temperatures from 5 to 80 °C, as shown in Fig. 5(a). The spectrum at each temperature was fitted using four Voigt profiles, as illustrated in Fig. 4(a). The individual fitting results at several selected temperatures are shown in Fig. S2 (ESI†). The obtained integral intensity ratios between *t*-configured and *g*-configured conformers were plotted as a function of temperature, as presented in Fig. 5(b). From Fig. 5(b), it can be seen that the relative intensity ratio decreases slowly as the temperature increases, from 0.83 at 5.0 °C to 0.71 at 80.0 °C, indicating that *t*-configured conformers are slightly more stable than *g*-configured ones in pure liquid *n*-propanol. Thus, like in the gas phase, the *n*-propanol molecule prefers a *trans*-OH conformation in pure liquid state. This is much different from the shorter chain ethanol molecule. Isolated ethanol has two conformers, corresponding to the OH group with *gauche* and *trans* configurations. Almost all previous studies agree that it favors the *trans*-OH state in the gas phase, whereas in the liquid state, it prefers a *gauche*-OH state according to studies using the neutron scattering technique and the dimer structures formed in supersonic relaxation experiments.[64,65] A straightforward interpretation for this difference may be that the carbon chain of the *n*-propanol molecule is longer than that of ethanol, and the adoption of *trans*-OH structures is favorable to reduce steric hindrance when forming hydrogen-bond chains or rings in liquid *n*-propanol. To the best of our knowledge, the preferred orientation of OH group in pure liquid *n*-propanol has not been determined previously. Combining our result with those of neutron scattering and X-ray diffraction techniques, it can be suggested that, like in the gas phase, the $G_t$ conformer is the most stable in pure liquid *n*-propanol.

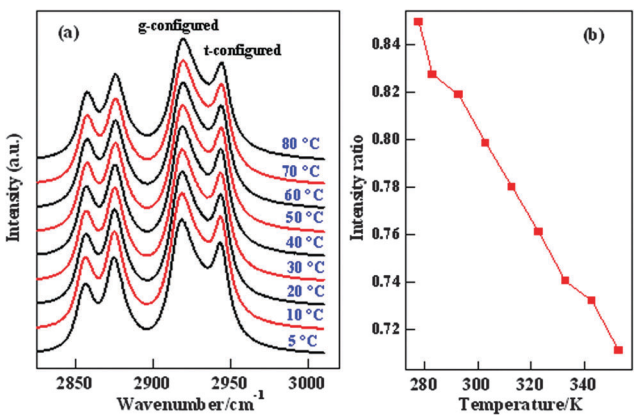


Fig. 5 (a) Observed temperature-dependent Raman spectra of pure liquid $CD_3CH_2CD_2OH$ in the C–H stretching region from 5 to 80 °C. (b) The dependence of relative intensity ratio between the *t*-configured and *g*-configured conformers on temperature (K) in liquid $CD_3CH_2CD_2OH$.

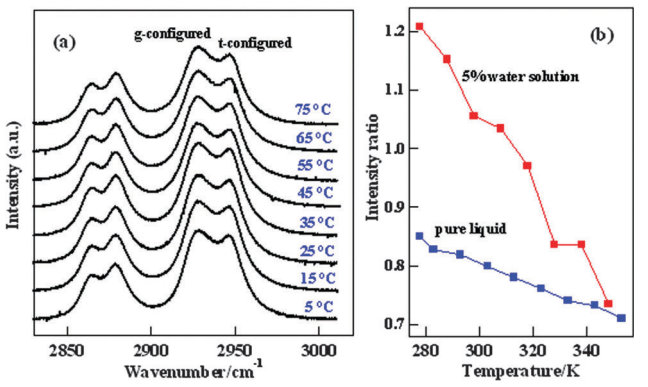


Fig. 6 (a) Observed temperature-dependent Raman spectra of liquid $CD_3CH_2CD_2OH$ in 5% water solution. (b) Relative intensity ratio between the *t*-configured and *g*-configured *n*-propanol conformers in 5% water solution *versus* temperature (K), along with those results for pure liquid *n*-propanol.

### Conformation of *n*-propanol in dilute aqueous solution

In addition to the investigations on the conformations of *n*-propanol molecules in gaseous and pure liquid states, much attention has been paid to the microscopic structure of aqueous *n*-propanol solutions since water plays an important role in various fields and detailed information on the structure of small organic molecules in water solution is helpful to understand the role of water in more complicated biological systems.[45,63,66]

Fig. 6(a) shows Raman spectra of $CD_3CH_2CD_2OH$ in 5% water solution recorded at temperature ranging from 5 to 75 °C. The individual fitting results at several selected temperatures are shown in Fig. S3 (ESI†). The relative integral intensity ratios between *t*-configured and *g*-configured conformers as a function of temperature are shown in Fig. 6(b), along with those results for pure liquid state in the same temperature range. It is evident that the relative intensity ratio also decreases in 5% *n*-propanol–water solution with increasing temperature, but the rate of decrease is much faster than in pure liquid state. This indicates that *n*-propanol molecules also prefer the *trans*-OH group in dilute aqueous solution, but this preference is enhanced compared with pure liquid state. That is to say, the water molecules play a role of further stabilizing the *trans*-OH *n*-propanol conformers. This will lead to conformational evolution from pure liquid to aqueous solution where *n*-propanol molecules with *gauche*-OH structure are transferred to the *trans*-OH structure when diluted with water, as shown in Fig. 7.

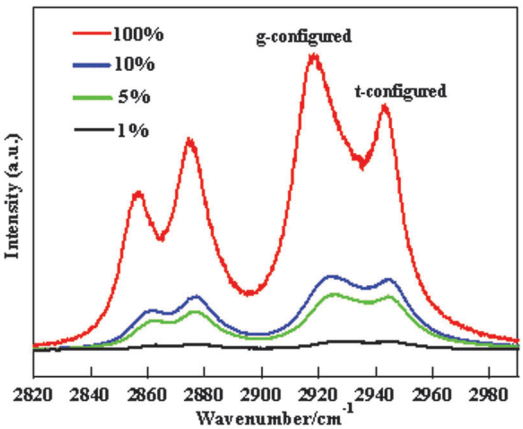


Fig. 7 Raman spectra of liquid $CD_3CH_2CD_2OH$ in water solutions of different concentration with *n*-propanol mole fraction of 100%, 10%, 5% and 1% (from top to bottom).

Fig. 7 presents Raman spectra of $CD_3CH_2CD_2OH$ in the C–H stretching region, measured for pure liquid (100%) and dilute water mixtures with *n*-propanol mole fraction of 10%, 5% and 1%. Fig. 8 shows the individual fitting results at each concentration, and Table 4 summarizes their relative integral intensity ratios between *t*-configured and *g*-configured conformers. It can be seen that relative intensity ratio is increased with increasing water concentration, indicating that the populations of *trans*-OH *n*-propanol conformers are increased as water concentrations increase. This observation agrees well with the conformational stability of *n*-propanol measured in pure liquid and in dilute water solution. According to a recent study on *n*-propanol–water mixtures by the large-angle X-ray scattering technique, when the mole fraction of *n*-propanol decreases to 10%, the tetrahedral-like structure of water predominates and *n*-propanol molecules are hydrated in the water structure.[63] Thus, the enhanced stability of *trans*-OH conformation in dilute *n*-propanol–water mixtures deserves further theoretical studies to elucidate how the water molecules influence *n*-propanol conformations. In addition, the experimental results for the small organic molecule presented here can serve as a benchmark for quantum dynamics calculations since it is still a challenge to accurately predict the properties in liquid or solution states.

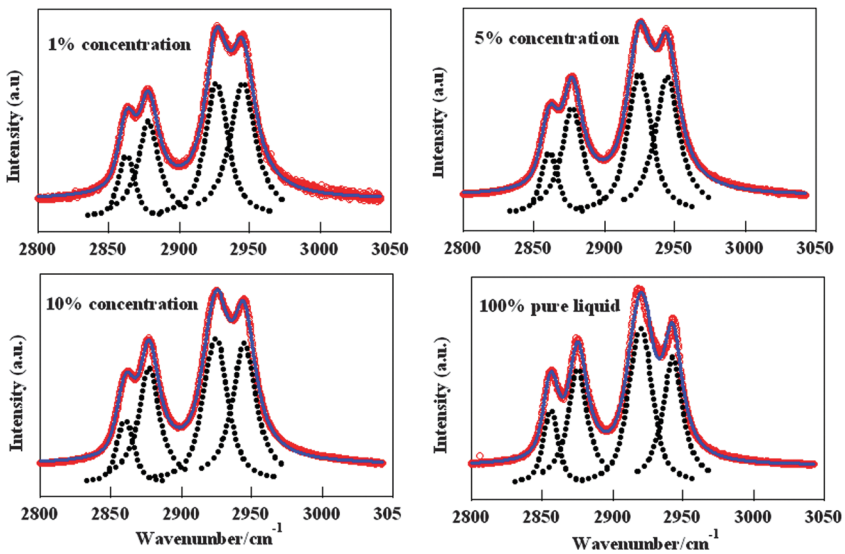


Fig. 8 The fitting result of Raman spectra of liquid $CD_3CH_2CD_2OH$ at each water concentration.

 

Table 4 The relative intensity ratio between *t*-configured and *g*-configured conformers of $CD_3CH_2CD_2OH$ in aqueous solutions of different concentration

| *n*-Propanol concentration | Intensity ratio |
|---|---|
| 100% | 0.81 |
| 10% | 1.07 |
| 5% | 1.11 |
| 1% | 1.21 |

## Conclusions

In this study, the gas-phase Raman spectra of deuterated *n*-propanol ($CD_3CH_2CD_2OH$) allowed, for the first time, unequivocal identification of all of its five conformers $T_t$, $G_t$, $G_{g'}$, $T_g$ and $G_g$ in the C–H stretching region, exhibiting sensitivity of site-specific C–H stretching vibration toward the molecular conformation. Assignment of the observed spectra to a particular conformer was facilitated by depolarization ratio measurement and quantum chemical calculations carried out at DFT (B3LYP) level of theory. The Raman spectra of liquid $CD_3CH_2CD_2OH$ in the C–H stretching region were analyzed on the basis of assignment in the gas phase. The results show that, like in the gas phase, the *n*-propanol molecules prefer a *trans*-OH structure in both pure liquid state and dilute aqueous solution, but this preference is further enhanced in the latter. This leads to conformational change from pure liquid state to dilute aqueous solution where *n*-propanol molecules of *gauche*-OH structure are transferred to *trans*-OH structure as water concentrations increase. The results provide important information on the microstructure of *n*-propanol in the liquid states, and demonstrate the potential of the C–H stretching vibration as a conformational probe in different environments. This is especially important when considering that C–H groups are ubiquitous in organic and biological molecules. The results presented here will shed new light on other molecules containing C–H groups.

## Acknowledgements

The present work was supported financially by the National Natural Science Foundation of China (NSFC, 20903002, 21273211, 21573208) and Anhui Provincial Natural Science Foundation (1408085MA18), Anhui Provincial Educational Ministry (KJ2015A040) and National Key Basic Research Special Foundation (NKBRSF, 2013CB834602).

## References

1 A. Sharma, I. Reva, R. Fausto, S. Hesse, Z. F. Xue, M. A. Suhm, S. K. Nayak, R. Sathishkumar, R. Pal and T. N. G. Row, *J. Am. Chem. Soc.*, 2011, **133**, 20194–20207.
2 R. Karaminkov, S. Chervenkov and H. J. Neusser, *J. Phys. Chem. A*, 2008, **112**, 839–848.
3 T. V. Nguyen, T. M. Korter and D. W. Pratt, *Mol. Phys.*, 2005, **103**, 1603–1613.
4 V. A. Shubert, D. Schmitz, C. Medcraft, A. Krin, D. Patterson, J. M. Doyle and M. Schnell, *J. Chem. Phys.*, 2015, **142**, 214201.
5 E. M. M. Tan, S. Amirjalayer, S. Smolarek, A. Vdovin, A. M. Rijs and W. J. Buma, *J. Phys. Chem. B*, 2013, **117**, 4798–4805.
6 B. Yan, S. Jaeqx, W. J. van der Zande and A. M. Rijs, *Phys. Chem. Chem. Phys.*, 2014, **16**, 10770–10778.
7 J. R. Clarkson, B. C. Dian, L. Moriggi, A. DeFusco, V. McCarthy, K. D. Jordan and T. S. Zwier, *J. Chem. Phys.*, 2005, **122**, 214311.
8 J. R. Carney and T. S. Zwier, *J. Phys. Chem. A*, 2000, **104**, 8677–8688.
9 T. A. LeGreve, E. E. Baquero and T. S. Zwier, *J. Am. Chem. Soc.*, 2007, **129**, 4028–4038.
10 N. Mayorkas, I. Malka and I. Bar, *Phys. Chem. Chem. Phys.*, 2011, **13**, 6808–6815.
11 A. Golan, N. Mayorkas, S. Rosenwaks and I. Bar, *J. Chem. Phys.*, 2009, **131**, 024305.
12 N. Mayorkas, S. Izbitski, A. Bernat and I. Bar, *J. Phys. Chem. Lett.*, 2012, **3**, 603–607.
13 N. Mayorkas, A. Bernat, S. Izbitski and I. Bar, *J. Chem. Phys.*, 2013, **138**, 124312.
14 T. V. Nguyen and D. W. Pratt, *J. Chem. Phys.*, 2006, **124**, 054317.
15 D. Patterson, M. Schnell and J. M. Doyle, *Nature*, 2013, **497**, 475–477.
16 C. Murli, N. Lu, Z. H. Dong and Y. Song, *J. Phys. Chem. B*, 2012, **116**, 12574–12580.
17 N. Y. Hu, K. Lin, X. G. Zhou and S. L. Liu, *Chin. J. Chem. Phys.*, 2015, **28**, 245–252.
18 B. T. G. Lutz, M. H. Langoor and J. H. van der Maas, *Vib. Spectrosc.*, 1998, **18**, 111–121.
19 P. J. Krueger and H. D. Mettee, *Can. J. Chem.*, 1964, **42**, 347–352.
20 R. G. Snyder, A. L. Aljibury, H. L. Strauss, H. L. Casal, K. M. Gough and W. F. Murphy, *J. Chem. Phys.*, 1984, **81**, 5352–5361.
21 R. A. Macphail, H. L. Strauss, R. G. Snyder and C. A. Elliger, *J. Phys. Chem.*, 1984, **88**, 334–341.
22 R. G. Snyder, H. L. Strauss and C. A. Elliger, *J. Phys. Chem.*, 1982, **86**, 5145–5150.
23 E. L. Sibert, N. M. Kidwell and T. S. Zwier, *J. Phys. Chem. B*, 2014, **118**, 8236–8245.
24 E. L. Sibert, *Mol. Phys.*, 2013, **111**, 2093–2099.
25 E. G. Buchanan, E. L. Sibert and T. S. Zwier, *J. Phys. Chem. A*, 2013, **117**, 2800–2811.
26 E. G. Buchanan, J. C. Dean, T. S. Zwier and E. L. Sibert, *J. Chem. Phys.*, 2013, **138**, 064308.
27 R. Lu, W. Gan, B. H. Wu, Z. Zhang, Y. Guo and H. F. Wang, *J. Phys. Chem. B*, 2005, **109**, 14118–14129.
28 N. G. Mirkin and S. Krimm, *Biopolymers*, 2010, **93**, 1065–1071.
29 N. G. Mirkin and S. Krimm, *Biopolymers*, 2009, **91**, 791–800.
30 C. S. Miller, E. A. Ploetz, M. E. Cremeens and S. A. Corcelli, *J. Chem. Phys.*, 2009, **130**, 125103.
31 N. G. Mirkin and S. Krimm, *J. Phys. Chem. A*, 2007, **111**, 5300–5303.
32 L. M. Imanov, A. A. Abdurakh and R. A. Ragimova, *Opt. Spectrosc. – USSR*, 1967, **22**, 456.

33 L. M. Imanov, A. A. Abdurakh and R. A. Ragimova, *Opt. Spectrosc. – USSR*, 1968, **25**, 528.
34 A. A. Abdurakhmanov, E. I. Veliyulin, R. A. Ragimova and L. M. Imanov, *J. Struct. Chem.*, 1981, **22**, 28–33.
35 Z. H. Luo, C. G. Ning, K. Liu, Y. R. Huang and J. K. Deng, *J. Phys. B: At., Mol. Opt. Phys.*, 2009, **42**, 165205.
36 Z. Kisiel, O. Dorosh, A. Maeda, I. R. Medvedev, F. C. De Lucia, E. Herbst, B. J. Drouin, J. C. Pearson and S. T. Shipman, *Phys. Chem. Chem. Phys.*, 2010, **12**, 8329–8339.
37 T. Haber, U. Schmitt and M. A. Suhm, *Phys. Chem. Chem. Phys.*, 1999, **1**, 5573–5582.
38 Y. L. Liu, S. C. Xu, L. Zhang, Y. Xu, B. Jiang, G. H. Sha, C. H. Zhang and J. C. Xie, *Chin. J. Chem. Phys.*, 2000, **13**, 513–520.
39 S. Jarmelo, N. Maiti, V. Anderson, P. R. Carey and R. Fausto, *J. Phys. Chem. A*, 2005, **109**, 2069–2077.
40 K. Kahn and T. C. Bruice, *ChemPhysChem*, 2005, **6**, 487–495.
41 T. N. Wassermann, P. Zielke, J. J. Lee, C. Cezard and M. A. Suhm, *J. Phys. Chem. A*, 2007, **111**, 7437–7448.
42 T. N. Wassermann, M. A. Suhm, P. Roubin and S. Coussan, *J. Mol. Struct.*, 2012, **1025**, 20–32.
43 A. Sahoo, S. Sarkar, P. S. R. Krishna, V. Bhagat and R. N. Joarder, *Pramana – J. Phys.*, 2008, **71**, 133–141.
44 A. Sahoo, S. Sarkar, V. Bhagat and R. N. Joarder, *J. Phys. Chem. A*, 2009, **113**, 5160–5162.
45 H. J. Tong, J. Y. Yu, Y. H. Zhang and J. P. Reid, *J. Phys. Chem. A*, 2010, **114**, 6795–6802.
46 Y. J. Jin, Y. Q. Yu, Y. X. Wang, K. Lin, X. G. Zhou and S. L. Liu, *Chin. J. Chem. Phys.*, 2015, **28**, 17–20.
47 Y. Q. Yu, K. Lin, X. G. Zhou, H. Wang, S. L. Liu and X. X. Ma, *J. Raman Spectrosc.*, 2007, **38**, 1206–1211.
48 Y. Q. Yu, K. Lin, X. G. Zhou, H. Wang, S. L. Liu and X. X. Ma, *J. Phys. Chem. C*, 2007, **111**, 8971–8978.
49 Y. Q. Yu, Y. X. Wang, N. Y. Hu, K. Lin, X. G. Zhou and S. L. Liu, *J. Raman Spectrosc.*, 2014, **45**, 259–265.
50 Y. Q. Yu, Y. X. Wang, K. Lin, N. Y. Hu, X. G. Zhou and S. L. Liu, *J. Phys. Chem. A*, 2013, **117**, 4377–4384.
51 M. Epshtein, A. Portnov, N. Mayorkas, S. Rosenwaks, B. Brauer and I. Bar, *J. Phys. Chem. A*, 2013, **117**, 11618–11623.
52 C. K. N. Patel and A. C. Tam, *Appl. Phys. Lett.*, 1979, **34**, 760–763.
53 J. J. Barrett and M. J. Berry, *Appl. Phys. Lett.*, 1979, **34**, 144–146.
54 K. Lin, X. G. Zhou, Y. Luo and S. L. Liu, *J. Phys. Chem. B*, 2010, **114**, 3567–3573.
55 K. Lin, N. Y. Hu, X. G. Zhou, S. L. Liu and Y. Luo, *J. Raman Spectrosc.*, 2012, **43**, 82–88.
56 L. Chen, W. D. Zhu, K. Lin, N. Y. Hu, Y. Q. Yu, X. G. Zhou, L. F. Yuan, S. M. Hu and Y. Luo, *J. Phys. Chem. A*, 2015, **119**, 3209–3217.
57 M. J. Frish, *et al.*, GAUSSIAN 09 (Reversion B.01), Gaussian, Inc., Pittsburgh, 2009.
58 J. M. L. Martin and C. V. Alsenoy, *GAR2PED*, University of Antwerp, Belgium, 1995.
59 P. L. Polavarapu, *J. Phys. Chem.*, 1990, **94**, 8106–8112.
60 P. Zielke and M. A. Suhm, *Phys. Chem. Chem. Phys.*, 2006, **8**, 2826–2830.
61 S. D. Williams, T. J. Johnson, T. P. Gibbons and C. L. Kitchens, *Theor. Chem. Acc.*, 2007, **117**, 283–290.
62 V. Barone, M. Biczysko and J. Bloino, *Phys. Chem. Chem. Phys.*, 2014, **16**, 1759–1787.
63 T. Takamuku, H. Maruyama, K. Watanabe and T. Yamaguchi, *J. Solution Chem.*, 2004, **33**, 641–660.
64 M. A. Gonzalez, E. Enciso, F. J. Bermejo and M. Bee, *Phys. Rev. B: Condens. Matter Mater. Phys.*, 2000, **61**, 6654–6666.
65 T. N. Wassermann and M. A. Suhm, *J. Phys. Chem. A*, 2010, **114**, 8223–8233.
66 P. Sillren, J. Swenson, J. Mattsson, D. Bowron and A. Matic, *J. Chem. Phys.*, 2013, **138**, 214501.

 